Supplemental information

PDGF Signaling Inhibits Mitophagy in Glioblastoma Stem Cells through N^6-methyladenosine

Deguan Lv, Ryan C. Gimple, Cuiqing Zhong, Qiulian Wu, Kailin Yang, Briana C. Prager, Bhaskar Godugu, Zhixin Qiu, Linjie Zhao, Guoxin Zhang, Deobrat Dixit, Derrick Lee, Jia Shen, Xiqing Li, Qi Xie, Xiuxing Wang, Sameer Agnihotri, Jeremy N. Rich

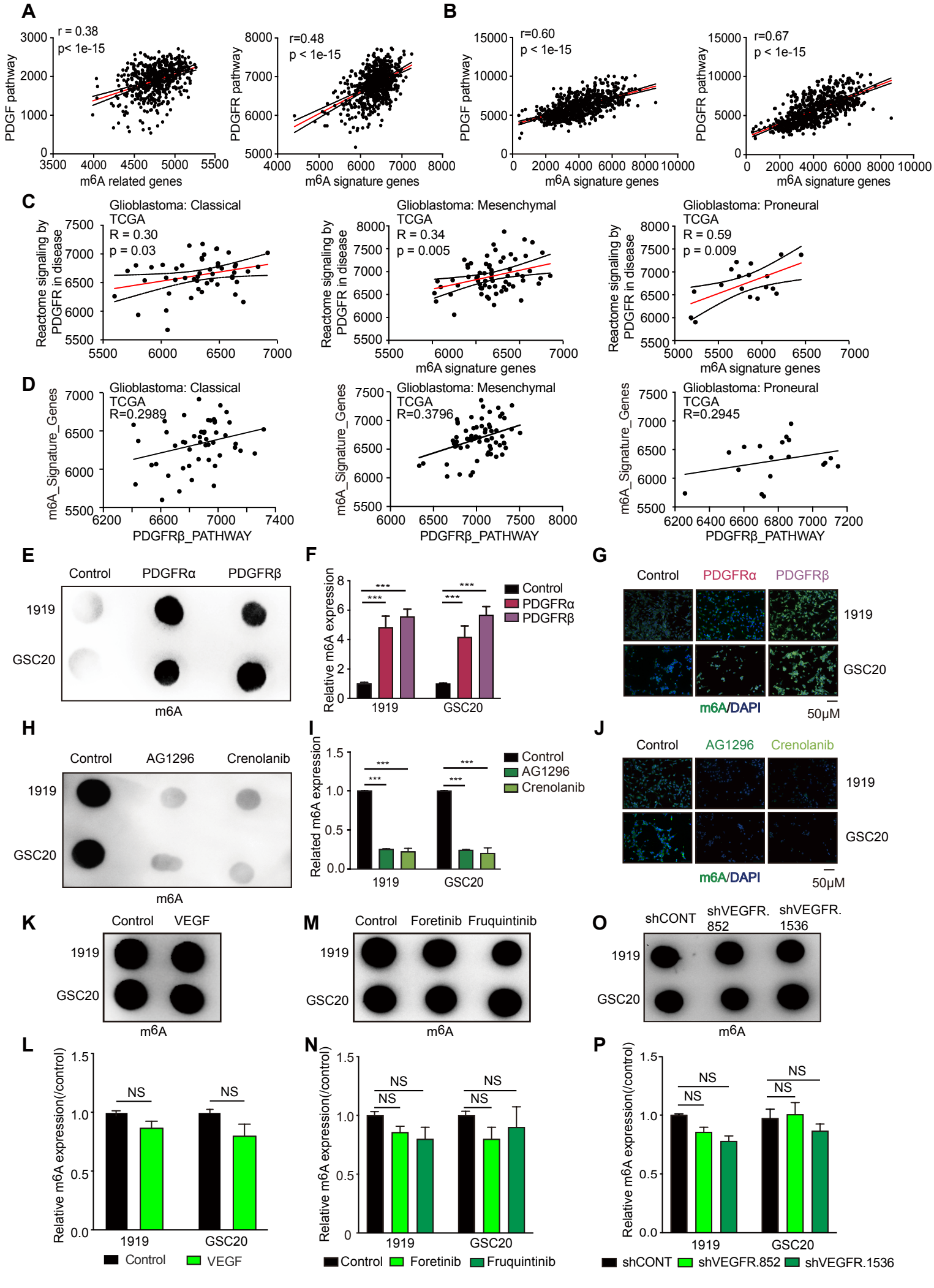
A
r = 0.38
p< 1e-15
PDGF pathway
m6A related genes
r=0.48
p < 1e-15
PDGFR pathway
m6A signature genes
B
r=0.60
p < 1e-15
PDGF pathway
m6A signature genes
r=0.67
p < 1e-15
PDGFR pathway
m6A signature genes
C
Glioblastoma: Classical
TCGA
R = 0.30
p = 0.03
Reactome signaling by PDGFR in disease
Glioblastoma: Mesenchymal
TCGA
R = 0.34
p = 0.005
m6A signature genes
Glioblastoma: Proneural
TCGA
R = 0.59
p = 0.009
m6A signature genes
D
Glioblastoma: Classical
TCGA
R=0.2989
m6A_Signature_Genes
PDGFRβ_PATHWAY
Glioblastoma: Mesenchymal
TCGA
R=0.3796
m6A_Signature_Genes
PDGFRβ_PATHWAY
Glioblastoma: Proneural
TCGA
R=0.2945
m6A_Signature_Genes
PDGFRβ_PATHWAY
E
Control
PDGFRα
PDGFRβ
1919
GSC20
m6A
F
Relative m6A expression
Control
PDGFRα
PDGFRβ
1919
GSC20
G
Control
PDGFRα
PDGFRβ
1919
GSC20
m6A/DAPI
50μM
H
Control
AG1296
Crenolanib
1919
GSC20
m6A
I
Related m6A expression
Control
AG1296
Crenolanib
1919
GSC20
J
Control
AG1296
Crenolanib
1919
GSC20
m6A/DAPI
50μM
K
Control
VEGF
1919
GSC20
m6A
M
Control
Foretinib
Fruquintinib
1919
GSC20
m6A
O
shCONT
shVEGFR. 852
shVEGFR. 1536
1919
GSC20
m6A
L
Relative m6A expression(/control)
NS
1919
GSC20
Control
VEGF
N
Relative m6A expression(/control)
NS
1919
GSC20
Control
Foretinib
Fruquintinib
P
Relative m6A expression(/control)
NS
1919
GSC20
shCONT
shVEGFR.852
shVEGFR.1536

Figure S1. VEGF signaling does not affect m^{6}A abundance in GSCs, related to Figure 1

(A) PDGF (left) and PDGFR (right) signaling positively corelates with m^{6}A signature in glioblastoma from TCAG dataset. (B) PDGF (left) and PDGFR (right) signaling positively corelates with m^{6}A signature in glioblastoma from CGGA dataset. (C) PDGFR signaling positively corelates with m^{6}A signature in different glioblastoma subtypes from TCGA dataset. (D) Correlative analysis was performed on the TCGA glioblastoma dataset with PDGFRB mRNA levels and an m^{6}A regulator signature in different glioblastoma subtypes. (E-G) PDGFR overexpression increases global m^{6}A levels in GSC. Verification of the m^{6}A abundance in GSC RNA by dot blot (E), colorimetric estimation (F) and immunofluorescence (G). (H-J) PDGFR inhibitors treatment decreases global m^{6}A levels in GSC. Verification of the m^{6}A abundance in GSC RNA by dot blot (H), colorimetric estimation (I) and immunofluorescence (J). (K and L) VEGF treatment has no effects on RNA global m^{6}A levels in GSC. Verification of the m^{6}A abundance in GSC RNA by dot blot (K), colorimetric estimation (L). (M and N) Global m^{6}A levels of RNA assay in GSC after VEGFR inhibitors treatment. Verification of the m^{6}A abundance in GSC RNA by dot blot (M), colorimetric estimation (N). (O and P) Global m^{6}A levels of RNA assay in GSC with VEGFR2 knockdown (shVEGFR2.852, shVEGFR2.1536). Verification of the m^{6}A abundance in GSC RNA by dot blot (O), colorimetric estimation (P).

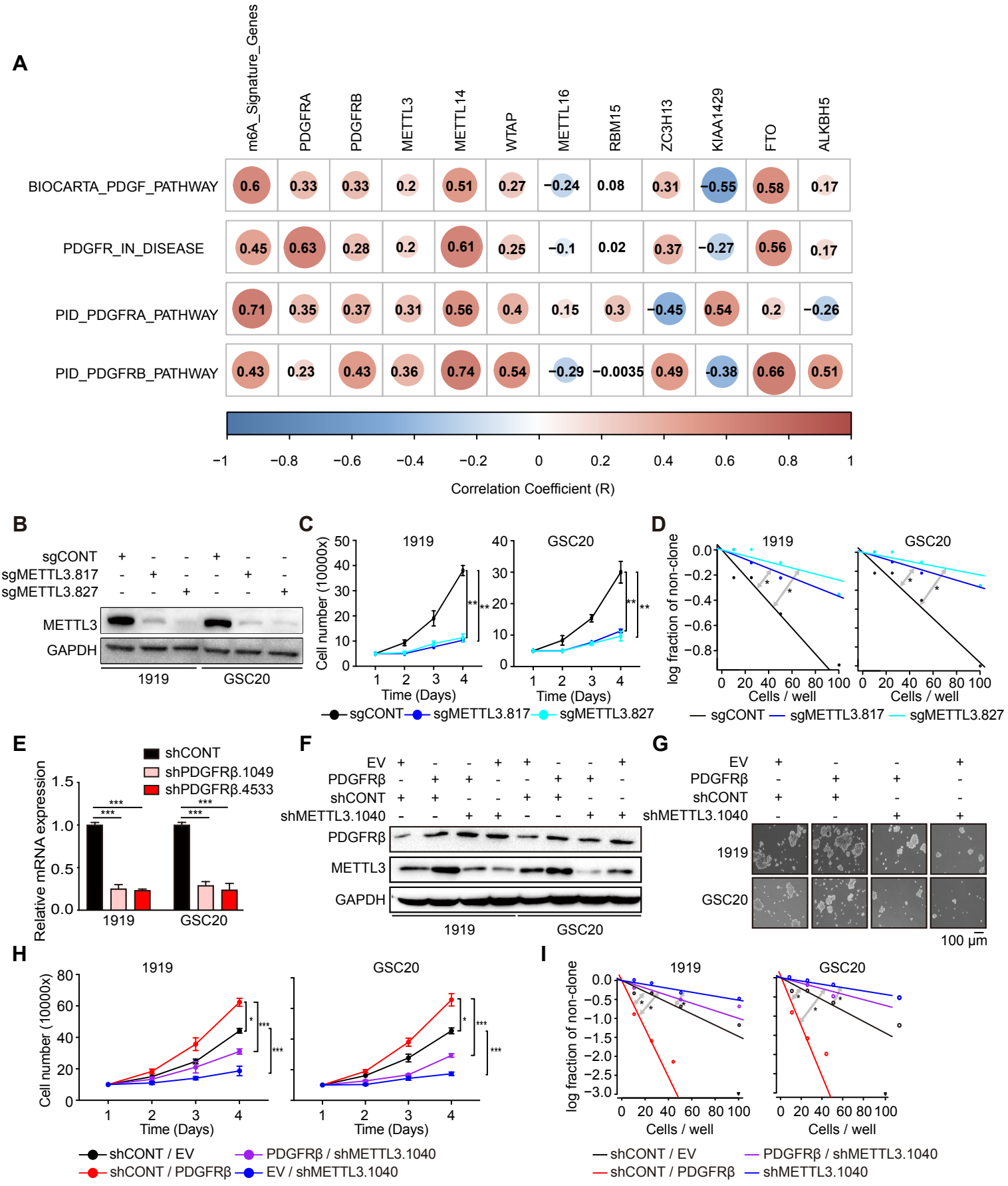
A
m6A_Signature_Genes
PDGFRA
PDGFRB
METTL3
METTL14
WTAP
METTL16
RBM15
ZC3H13
KIAA1429
FTO
ALKBH5
BIOCARTA_PDGF_PATHWAY 0.6 0.33 0.33 0.2 0.51 0.27 −0.24 0.08 0.31 −0.55 0.58 0.17
PDGFR_IN_DISEASE 0.45 0.63 0.28 0.2 0.61 0.25 −0.1 0.02 0.37 −0.27 0.56 0.17
PID_PDGFRA_PATHWAY 0.71 0.35 0.37 0.31 0.56 0.4 0.15 0.3 −0.45 0.54 0.2 −0.26
PID_PDGFRB_PATHWAY 0.43 0.23 0.43 0.36 0.74 0.54 −0.29 −0.0035 0.49 −0.38 0.66 0.51
−1 −0.8 −0.6 −0.4 −0.2 0 0.2 0.4 0.6 0.8 1
Correlation Coefficient (R)
B
sgCONT
sgMETTL3.817
sgMETTL3.827
METTL3
GAPDH
1919
GSC20
C
1919
GSC20
Cell number (10000x)
Time (Days)
sgCONT
sgMETTL3.817
sgMETTL3.827
D
1919
GSC20
log fraction of non-clone
Cells / well
sgCONT
sgMETTL3.817
sgMETTL3.827
E
shCONT
shPDGFRβ.1049
shPDGFRβ.4533
Relative mRNA expression
1919
GSC20
F
EV
PDGFRβ
shCONT
shMETTL3.1040
PDGFRβ
METTL3
GAPDH
1919
GSC20
G
EV
PDGFRβ
shCONT
shMETTL3.1040
1919
GSC20
100 μm
H
1919
GSC20
Cell number (10000x)
Time (Days)
shCONT / EV
shCONT / PDGFRβ
PDGFRβ / shMETTL3.1040
EV / shMETTL3.1040
I
1919
GSC20
log fraction of non-clone
Cells / well
shCONT / EV
shCONT / PDGFRβ
PDGFRβ / shMETTL3.1040
shMETTL3.1040

Figure S2. METTL3 knockout impairs PDGF-induced GSCs proliferation and clone formation, related to Figure 2

(A) Correlations between PDGF/PDGFR signatures and various m^6A signature genes in CGGA datasets. (B) WB assays of METTL3 protein levels in 1919 and GSC20 cells following METTL3 knockout with two different sgMETTL3 (sgMETTL3.817, sgMETTL3.827) or a non-targeting sgRNA (sgCONT). (C) Cell viability of METTL3 knockout GSCs 1919 (left) and GSC20 (right), up to 3 days of post-transduction. **, $p < 0.01$. Error bars show standard deviation. (D) *In vitro* limiting dilution assay in 1919 (left) and GSC20 (right) following knockout with two independent sgRNAs targeting METTL3 or a non-targeting sgRNA (sgCONT). 10 wells were quantified for each condition and 3 biologic replicates for the assay. *, $p < 0.05$. (E) qPCR analysis of METTL3 mRNA expression following knockdown with two independent, non-overlapping shRNAs targeting PDGFRβ (shPDGFRβ.2164 and shPDGFRβ.2682) or a non-targeting shRNA (shCONT). Three technical replicates were used for each condition. Statistical significance was assessed using a two-way ANOVA with Sidak multiple test correction, ***, $p < 0.001$. (F) WB assays of METTL3 knockdown in 1919 and GSC20 cells with, or without PDGFRβ overexpression. (G) Spheres formation of 1919 and GSC20 following transduction with METTL3 knockdown (shMETTL3.915 and shMETTL3.1040) with or without PDGFRβ overexpression. (H) Cell viability of METTL3 knockdown GSCs, in the presence or absence of PDGFRβ overexpression, up to 3 days of post-transduction. Error bars show standard deviation. *, $p < 0.05$, ***, $p < 0.001$. (H) *In vitro* limiting dilution assay in 1919

and GSC20 following knockdown with two independent, non-overlapping shRNAs targeting METTL3 or a non-targeting shRNA (shCONT) with or without PDGFRβ overexpression. 10 wells were quantified for each condition and 3 biologic replicates for the assay. *, $p < 0.05$.

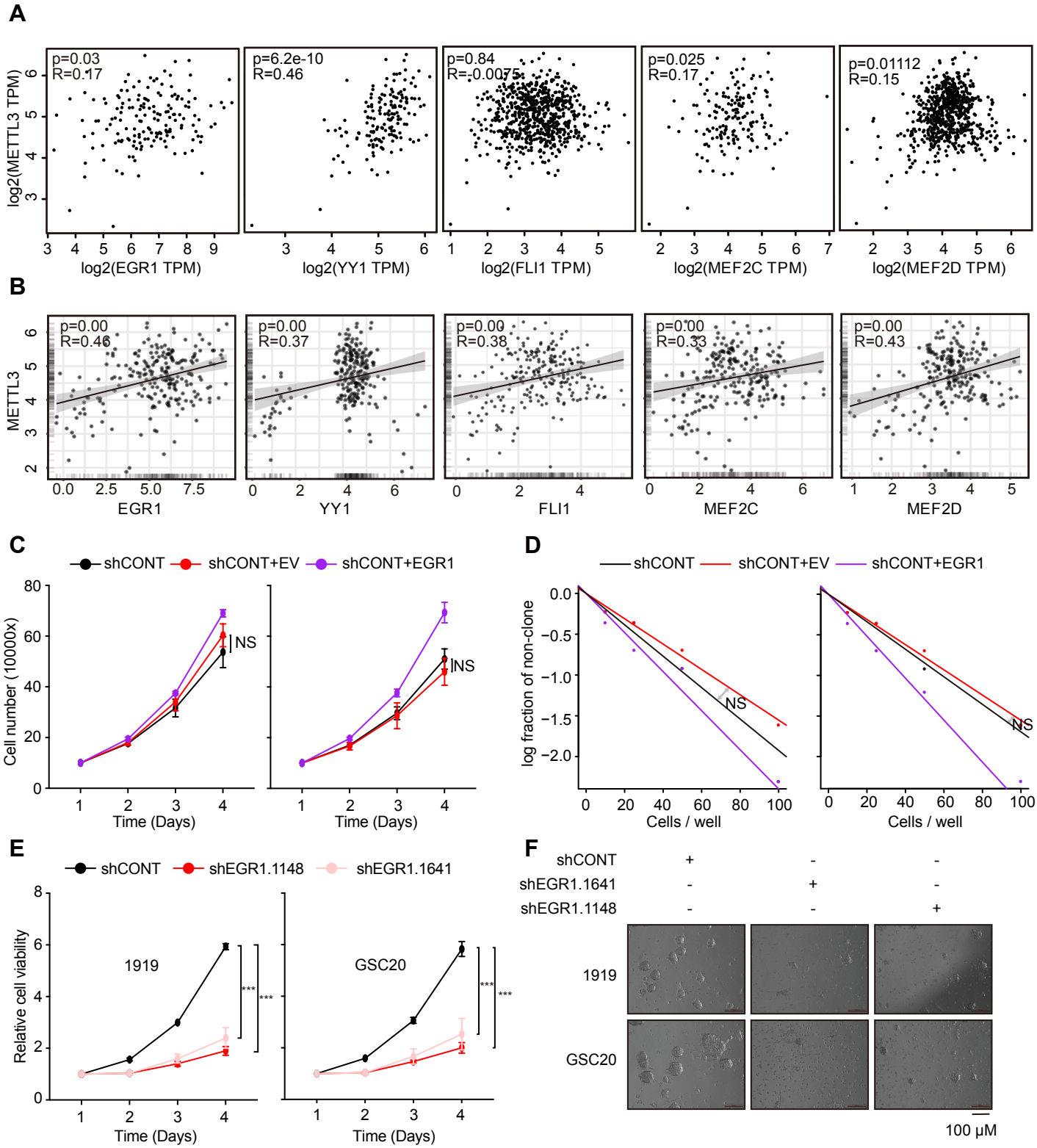
A
p=0.03
R=0.17
p=6.2e-10
R=0.46
p=0.84
R=-0.0075
p=0.025
R=0.17
p=0.01112
R=0.15
log2(METTL3 TPM)
log2(EGR1 TPM)
log2(YY1 TPM)
log2(FLI1 TPM)
log2(MEF2C TPM)
log2(MEF2D TPM)
B
p=0.00
R=0.46
p=0.00
R=0.37
p=0.00
R=0.38
p=0.00
R=0.33
p=0.00
R=0.43
METTL3
EGR1
YY1
FLI1
MEF2C
MEF2D
C
shCONT
shCONT+EV
shCONT+EGR1
Cell number (10000x)
NS
NS
Time (Days)
Time (Days)
D
shCONT
shCONT+EV
shCONT+EGR1
log fraction of non-clone
NS
NS
Cells / well
Cells / well
E
shCONT
shEGR1.1148
shEGR1.1641
Relative cell viability
1919
GSC20
***
***
***
***
Time (Days)
Time (Days)
F
shCONT + - -
shEGR1.1641 - + -
shEGR1.1148 - - +
1919
GSC20
100 μM

Figure S3. EGR1 is an oncogene in glioblastoma, related to Figure 3

(A and B) The correlation analysis of TFs and METTL3 with TCGA dataset (A) and CGGA dataset (B). (C) Cell viability of EV or EGR1-transduced GSCs 1919 and GSC20 in shCONT. NS, no statistical significance. Error bars show standard deviation. (D) In vitro limiting dilution assay in 1919 and GSC20 following overexpressed EV or EGR1 with non-targeting shRNA (shCONT) knockdown. 10 wells were quantified for each condition and 3 biologic replicates for the assay. NS, not statistically significant. (E) Cell viability in the 1919 (left) and GSC20 (right) cell models over a 3-day time course following knockdown with two independent, non-overlapping shRNAs targeting EGR1 (shEGR1.1641 and shEGR1.1148) or a non-targeting shRNA (shCONT). Three technical replicates were performed for each group. One-way ANOVA was used for statistical analysis with Dunnett's multiple hypothesis test correction with three technical replicates. ***, $p < 0.001$. (F) Functional assays of self-renewal (serial neurosphere passage), and tumor propagation using in vitro limiting dilution after EGR1 knockdown with two independent, non-overlapping shRNAs targeting EGR1 (shEGR1.1641 and shEGR1.1148) or a non-targeting shRNA (shCONT). Scale bar: 100μM.

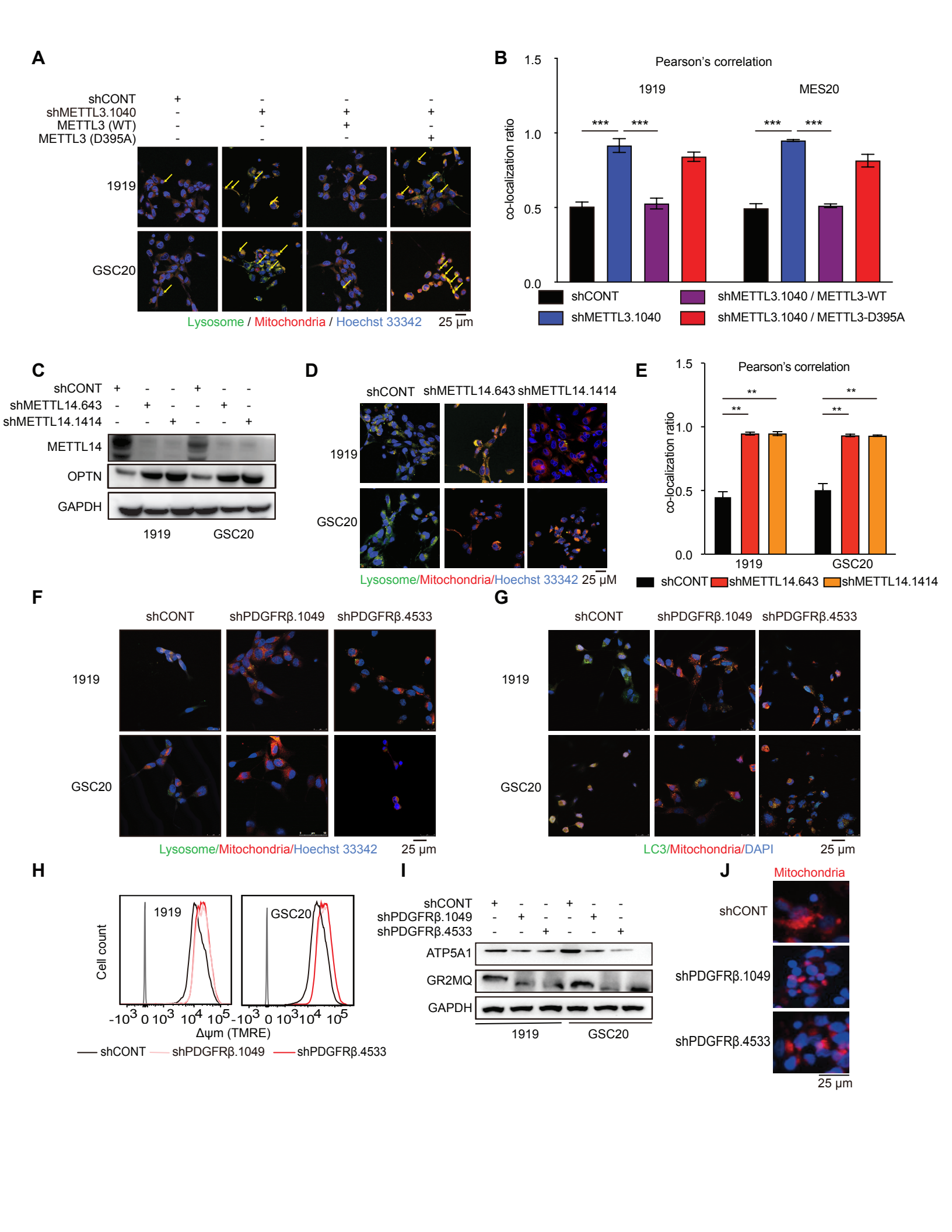
A
shCONT
shMETTL3.1040
METTL3 (WT)
METTL3 (D395A)
1919
GSC20
Lysosome / Mitochondria / Hoechst 33342
25 μm
B
Pearson's correlation
1919
MES20
co-localization ratio
shCONT
shMETTL3.1040
shMETTL3.1040 / METTL3-WT
shMETTL3.1040 / METTL3-D395A
C
shCONT
shMETTL14.643
shMETTL14.1414
METTL14
OPTN
GAPDH
1919
GSC20
D
shCONT
shMETTL14.643
shMETTL14.1414
1919
GSC20
Lysosome/Mitochondria/Hoechst 33342
25 μM
E
Pearson's correlation
co-localization ratio
1919
GSC20
shCONT
shMETTL14.643
shMETTL14.1414
F
shCONT
shPDGFRβ.1049
shPDGFRβ.4533
1919
GSC20
Lysosome/Mitochondria/Hoechst 33342
25 μm
G
shCONT
shPDGFRβ.1049
shPDGFRβ.4533
1919
GSC20
LC3/Mitochondria/DAPI
25 μm
H
1919
GSC20
Cell count
Δψm (TMRE)
shCONT
shPDGFRβ.1049
shPDGFRβ.4533
I
shCONT
shPDGFRβ.1049
shPDGFRβ.4533
ATP5A1
GR2MQ
GAPDH
1919
GSC20
J
Mitochondria
shCONT
shPDGFRβ.1049
shPDGFRβ.4533
25 μm

Figure S4. PDGFRβ affects mitochondrial function via mitophagy, related to Figure 4

(A) Cellular colocalization of lysosome and mitochondria in 1919 (above) and GSC20 (below) after shRNA-resistant METTL3 (WT) or (D395A) overexpression with, or without METTL3 knockdown (shMETTL3.1040) by immunofluorescence staining using lysosomal and mitochondrial probe. Yellow arrows designate mitochondria that are being degraded. Scale bar: 25 μm. (B) Pearson's correlation coefficient is shown in bar graph format from three independent experiments in METTL3 rescue GSCs. Error bars show standard deviation. ***, $p < 0.001$. (C) Two patient-derived GSCs, 1919 and GSC20, were transduced with either one of two non-overlapping shRNAs targeting METTL14 or shCONT. WB assays of METTL14 and OPTN protein levels were performed. (D) Cellular colocalization of lysosome and mitochondria in 1919 (top) and GSC20 (bottom) after METTL14 knockdown, as demonstrated by immunofluorescence staining using lysosomal and mitochondrial probes. Scale bar: 25 μm. (E) Pearson's correlation coefficient is shown in bar graph format for (D). Error bars represents the standard deviation. **, $p < 0.01$. (F) Cellular colocalization of lysosome and mitochondria in 1919 (left) and GSC20 (right) as demonstrated by immunofluorescence staining using lysosomal and mitochondrial probe. Scale bar: 25 μm. (G) Cellular colocalization and levels of LC3 and mitochondria in 1919 (left) and GSC20 (right) as demonstrated by immunofluorescence staining using LC3 antibody and mitochondrial probe. Scale bar: 25 μm. (H) PDGFRβ knockdown with two independent, non-overlapping shRNAs (shPDGFRβ.1049 and shPDGFRβ.4533) increases 1919 (left) and GSC20 (right) cell mitochondrial

membrane potential by flow cytometry analysis. (I) METTL3 knockdown with two independent, non-overlapping shRNAs (shPDGFRβ.1049 and shPDGFRβ.4533) decreases number of mitochondria in GSC1919. (J) PDGFRβ knockdown with two independent, non-overlapping shRNAs (shPDGFRβ.1049 and shPDGFRβ.4533) decreases number of mitochondria in GSC1919.

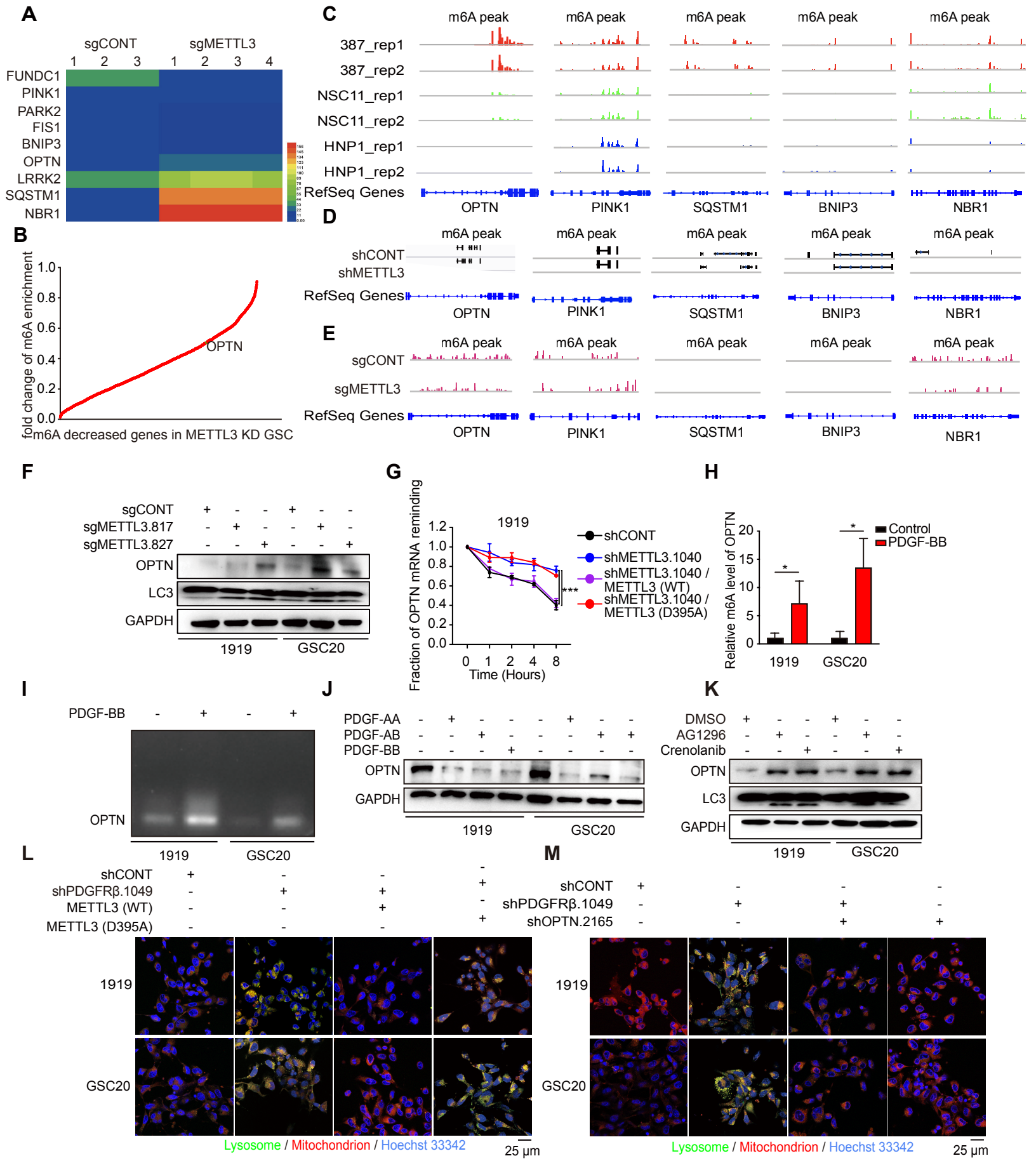
A
sgCONT
sgMETTL3
1 2 3 1 2 3 4
FUNDC1
PINK1
PARK2
FIS1
BNIP3
OPTN
LRRK2
SQSTM1
NBR1
B
fold change of m6A enrichment
1.0
0.8
0.6
0.4
0.2
0.0
OPTN
m6A decreased genes in METTL3 KD GSC
C
m6A peak
387_rep1
387_rep2
NSC11_rep1
NSC11_rep2
HNP1_rep1
HNP1_rep2
RefSeq Genes
OPTN
PINK1
SQSTM1
BNIP3
NBR1
D
shCONT
shMETTL3
RefSeq Genes
E
sgCONT
sgMETTL3
RefSeq Genes
F
sgCONT
sgMETTL3.817
sgMETTL3.827
OPTN
LC3
GAPDH
1919
GSC20
G
1919
Fraction of OPTN mRNA reminding
Time (Hours)
shCONT
shMETTL3.1040
shMETTL3.1040 / METTL3 (WT)
shMETTL3.1040 / METTL3 (D395A)
***
H
Relative m6A level of OPTN
Control
PDGF-BB
*
I
PDGF-BB
OPTN
1919
GSC20
J
PDGF-AA
PDGF-AB
PDGF-BB
OPTN
GAPDH
1919
GSC20
K
DMSO
AG1296
Crenolanib
OPTN
LC3
GAPDH
1919
GSC20
L
shCONT
shPDGFRβ.1049
METTL3 (WT)
METTL3 (D395A)
1919
GSC20
Lysosome / Mitochondrion / Hoechst 33342
25 μm
M
shCONT
shPDGFRβ.1049
shOPTN.2165
1919
GSC20
Lysosome / Mitochondrion / Hoechst 33342
25 μm

Figure S5. PDGF-METTL3 inhibits mitophagy via regulating OPTN m^{6}A modification in GSCs, related to Figure 5

(A) Heatmap of mitophagy related genes expression in METTL3 knockout cells. (B) m^{6}A abundance assay in GSC after METTL3 knockout. (C) m^{6}A signal of OPTN, PINK1, SQSTM1, BNIP3, and NBR1 in GSC and NSCs at the gene locus. (D and E) m^{6}A signal in OPTN locus after METTL3 knockout (D) and knockdown (E). (F) WB assays of OPTN and LC3 level in GSC with METTL3 knockout. (G) METTL3 promotes OPTN mRNA decay in GSCs. qPCR analysis of mRNA expression in 1919 after METTL3-WT or METTL3-mutant overexpression in METTL3 knockdown cell line treated with actinomycin D. Student's t-test with Holm-Sidak multiple test correction. ***, $p < 0.001$. (H) Verification of the m^{6}A abundance in 1919 and GSC20 RNA with PDGFRβ knockdown by MeRIP-qPCR. ***, $p < 0.001$. (I) Agarose gel image of MeRIP-qPCR result from H. (J) WB assays of OPTN expression in 1919 and GSC20 after PDGF treatment. (K) WB assays of LC3 and OPTN expression in 1919 and GSC20 after PDGFR inhibitors treatment. (L) Cellular colocalization of mitochondrion and lysosome in METTL3 WT or D395A rescued 1919 and GSC20 cells. Scale bar: 25 μm. (M) Cellular colocalization of lysosome and mitochondria in 1919 and GSC20 with PDGFβ and OPTN knockdown as demonstrated by immunofluorescence staining using lysosomal and mitochondrial probe. Scale bar: 25 μm.

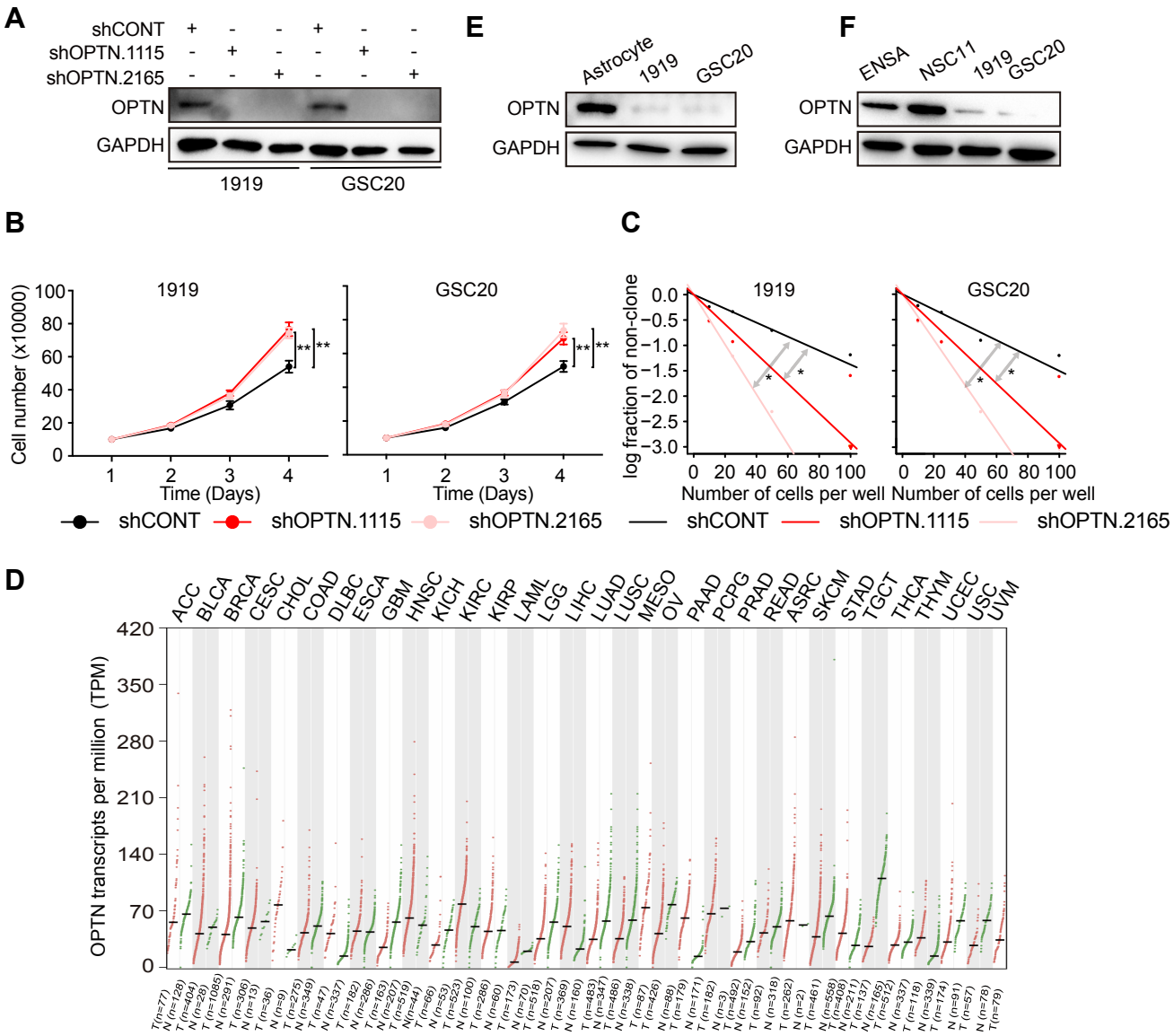
A
shCONT
shOPTN.1115
shOPTN.2165
OPTN
GAPDH
1919
GSC20
E
Astrocyte
1919
GSC20
OPTN
GAPDH
F
ENSA
NSC11
1919
GSC20
OPTN
GAPDH
B
1919
GSC20
Cell number (x10000)
Time (Days)
shCONT
shOPTN.1115
shOPTN.2165
C
1919
GSC20
log fraction of non-clone
Number of cells per well
shCONT
shOPTN.1115
shOPTN.2165
D
OPTN transcripts per million (TPM)
ACC BLCA BRCA CESC CHOL COAD DLBC ESCA GBM HNSC KICH KIRC KIRP LAML LGG LIHC LUAD LUSC MESO OV PAAD PCPG PRAD READ ASRC SKCM STAD TGCT THCA THYM UCEC USC UVM

Figure S6. OPTN is a novel suppressor in glioblastoma, related to Figure 6

(A) Cell viability of METTL3 knockdown GSCs, up to 3 days of post-transduction. Error bars show standard deviation. *, $p < 0.05$. (B) In vitro limiting dilution assay in 1919 and GSC20 following knockdown with two independent, non-overlapping shRNAs targeting OPTN or a non-targeting shRNA (shCONT). 10 wells were quantified for each condition and 3 biologic replicates for the assay. *, $p < 0.05$. (C) WB assays of OPTN expression following knockdown with two independent, non-overlapping shRNAs targeting OPTN (shOPTN.1115 and shOPTN.2165) or a non-targeting shRNA (shCONT). (D) Landscape of OPTN expression in pan-cancers. (E) WB assays of OPTN expression in astrocyte and GSCs. (F) WB assays of OPTN expression in NSCs (ENSA and NSC11) and GSCs.

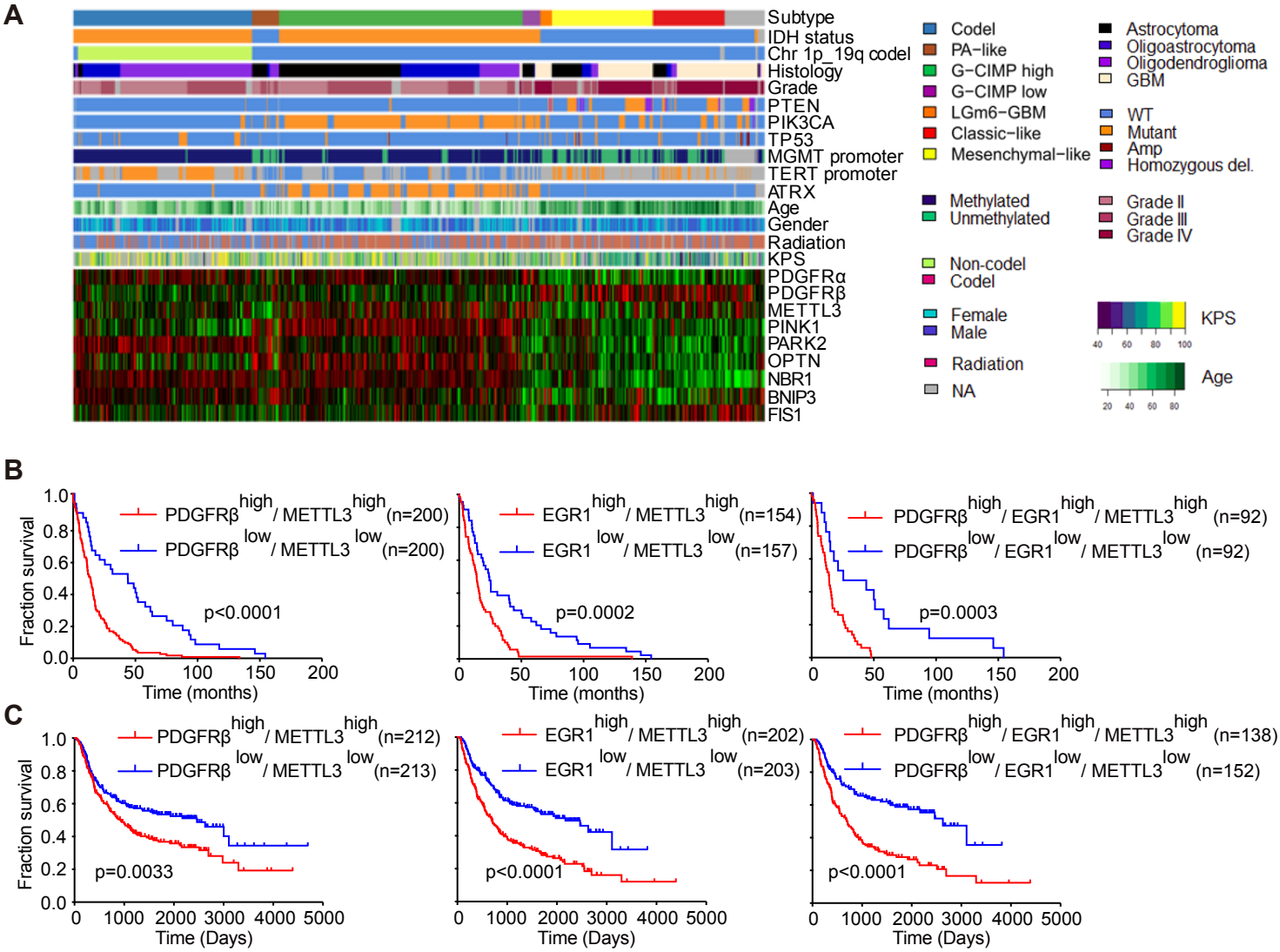
A
Subtype
IDH status
Chr 1p_19q codel
Histology
Grade
PTEN
PIK3CA
TP53
MGMT promoter
TERT promoter
ATRX
Age
Gender
Radiation
KPS
PDGFRα
PDGFRβ
METTL3
PINK1
PARK2
OPTN
NBR1
BNIP3
FIS1
Codel
PA-like
G-CIMP high
G-CIMP low
LGm6-GBM
Classic-like
Mesenchymal-like
Astrocytoma
Oligoastrocytoma
Oligodendroglioma
GBM
WT
Mutant
Amp
Homozygous del.
Methylated
Unmethylated
Grade II
Grade III
Grade IV
Non-codel
Codel
Female
Male
Radiation
NA
KPS
Age
B
Fraction survival
PDGFRβ high / METTL3 high (n=200)
PDGFRβ low / METTL3 low (n=200)
p<0.0001
Time (months)
EGR1 high / METTL3 high (n=154)
EGR1 low / METTL3 low (n=157)
p=0.0002
Time (months)
PDGFRβ high / EGR1 high / METTL3 high (n=92)
PDGFRβ low / EGR1 low / METTL3 low (n=92)
p=0.0003
Time (months)
C
Fraction survival
PDGFRβ high / METTL3 high (n=212)
PDGFRβ low / METTL3 low (n=213)
p=0.0033
Time (Days)
EGR1 high / METTL3 high (n=202)
EGR1 low / METTL3 low (n=203)
p<0.0001
Time (Days)
PDGFRβ high / EGR1 high / METTL3 high (n=138)
PDGFRβ low / EGR1 low / METTL3 low (n=152)
p<0.0001
Time (Days)

Figure S7. PDGF-EGR1-METTL3 axis is clinically prognostic, related to Figure 7

(A) Heatmaps of TCGA glioma samples displaying mRNA levels of PDGFRβ-METTL3 along with clinical and genetic variant information for each sample. (B) Kaplan-Meier curve showing patient survival based on PDGFRβ, EGR1 and METTL3 mRNA expression in glioma patients from the TCGA dataset. Log-rank test was used for statistical analysis. $PDGFR\beta^{high}$ $METTL3^{high}$ vs. $PDGFR\beta^{low}$ $METTL3^{low}$ ($p < 0.0001$), $EGR1^{high}$ $METTL3^{high}$ vs. $EGR1^{low}$ $METTL3^{low}$ ($p = 0.0002$), $PDGFR\beta^{high}$ $EGR1^{high}$ $METTL3^{high}$ vs. $PDGFR\beta^{low}$ $EGR1^{low}$ $METTL3^{low}$ ($p = 0.0003$). (C) Kaplan-Meier curve showing patient survival based on PDGFRβ, EGR1and METTL3 mRNA expression in glioma patients from the CGGA dataset. Log-rank test was used for statistical analysis. $PDGFR\beta^{high}$ $METTL3^{high}$ vs. $PDGFR\beta^{low}$ $METTL3^{low}$ ($p = 0.0033$), $EGR1^{high}$ $METTL3^{high}$ vs. $EGR1^{low}$ $METTL3^{low}$ ($p < 0.0001$), $PDGFR\beta^{high}$ $EGR1^{high}$ $METTL3^{high}$ vs. $PDGFR\beta^{low}$ $EGR1^{low}$ $METTL3^{low}$ ($p < 0.0001$). (D) The correlation analysis of PDGFR and METTL3, METTL3 and OPTN in breast invasive carcinoma, lung adenocarcinoma, colon adenocarcinoma, prostate adenocarcinoma, liver hepatocellular carcinoma, stomach adenocarcinoma, and glioblastoma with TCGA dataset. (E and F) WB assays of METTL3 and OPTN expression in A549, MD231, and HepG2 cells with or without PDGF and PDGFR inhibitors treatment. (G) WB assays of PDGFRB expression in A549, MD231, and HepG2 cells. (H) WB assays of METTL3 expression in GSC and DGC pairs derived from 1919 and GSC20 xenografts. (I) RNA m^6A methylation levels measured by colorimetric assay from RNA samples from 1919 and GSC20 GSCs and the differentiated glioma cells. (J) GSC 1919 and GSC20

differentiation decreases OPTN m^6A levels. Verification of the m^6A abundance in 1919 and GSC20 RNA by MeRIP-qPCR.